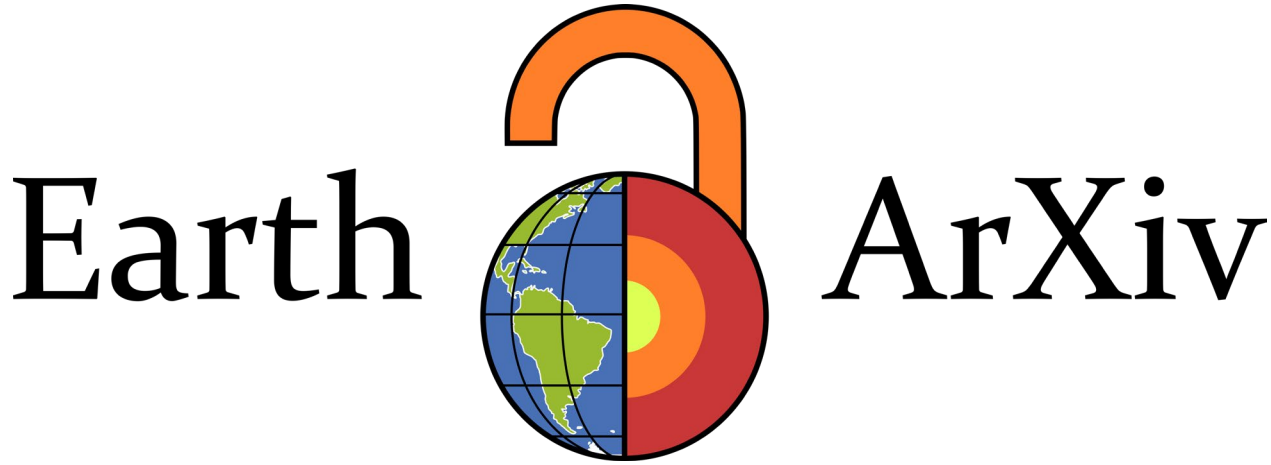

The software code and binaries are available at https://github.com/GeoSebastianStumpf/ICP-Base

ICP-Base: A free and open-source software solution for centralized LA-ICP-MS data processing, evaluation and management

Sebastian Stumpf[a*], Nils B. Gies[a], Thomas Pettke[a] and Marcel Guillong[b]

[a] Institute of Geological Sciences, University of Bern, 3012 Bern, Switzerland

[b] Department of Earth and Planetary Sciences, ETH Zürich, CH-8092 Zürich

*Corresponding author: sebastian.stumpf@unibe.ch

ABSTRACT

Transient signal intensity data, particularly since the advent of Laser Ablation–Inductively Coupled Plasma–Mass Spectrometry (LA-ICP-MS), have become a standard tool in petrology and geochemistry for determining the chemical composition of minerals and fluid and melt inclusions. However, commonly used software for quantifying raw ICP-MS data is often inflexible, expensive, and closed-source, typically providing only tabular output, leaving analytical data scattered across files and systems. ICP-Base is a free and open-source software featuring a graphical user interface designed to enhance transparency, versatility and efficiency in LA-ICP-MS data processing. It integrates raw data, processing parameters, results and metadata within a centralized hierarchical database, preserving the full analytical context and facilitating both short- and long-term evaluation and instrument monitoring. The software supports processing of mineral spot analyses, fully enclosed fluid and solid inclusions analyses, and line scan data. It introduces transparent approaches for host–inclusion signal deconvolution and enables sequential and parallel quantification using multiple external reference materials and highly flexible internal standardization approaches. All data processing, evaluation, and visualization are performed within the software environment, with visualization handled through integration of the VisModule from MinPlotX, enabling direct generation of publication-ready figures without relying on external tools. Owing to its modular design and availability of the source code, ICP-Base provides a flexible framework for community-driven development and future methodological expansion in LA-ICP-MS data processing.

Introduction

Quantitative microanalysis is fundamental to modern science including petrology, geochemistry and paleoclimatology, providing the chemical information necessary to investigate natural processes and materials. Among the available analytical techniques, Laser Ablation–Inductively Coupled Plasma–Mass Spectrometry (LA-ICP-MS) is one of the most widely used methods for *in-situ* elemental analysis.

The most common application of LA-ICP-MS systems is the spot analysis of homogeneous solids, which remains the fastest and most versatile method for major to trace element mass fraction data acquisition. Moreover, LA-ICP-MS is the most powerful technique for quantitative elemental and isotope ratio analysis of fluid and solid inclusions fully enclosed within minerals (Günther et al., 1998; Audétat et al., 1998; Halter et al., 2002; Heinrich et al., 2003; Pettke et al., 2012). The raw transient signals, which are often complex with rapidly changing intensities, require careful treatment and processing to ensure correct and reliable quantification. Most commonly used commercial software to quantify raw mass spectrometry data, e.g., Iolite, GLITTER and HDIP are often inflexible, expensive, and closed-source, limiting control on advanced data evaluation and processing and, more generally, impeding innovation. A variety of specialized, free, and open-source software packages are available for LA-ICP-MS data processing, such as TERMITE (Mischel et al., 2017), LAtools (Branson et al., 2019), Ilaps (Faltusová et al., 2022), G.O.Joe (Altenberger et al., 2024), and XMapTools (Lanari et al., 2014; Markmann et al., 2024). Some of these tools are script-based and lack a graphical user interface, and most focus solely on the quantification of mineral spot analyses and/or 2D imaging. For the quantification of single- and polyphase fluid and solid inclusions fully enclosed in host minerals, SILLS (Guillong et al., 2008) remains the most widely used and established software. However, it comes with several limitations: it supports only a narrow range of raw data formats, processes a single measurement bracket at a time, allows the use of only one external standard, and is no longer actively maintained. The deconvolution of host and inclusion signals offers limited transparency to the user even though the evaluation of this step is crucial to properly assess data credibility and quality.

Currently available software mostly provide only tabular output (e.g., spreadsheets), requiring users to laboriously evaluate, compare, and visualize their results in separate applications. This fragmentation highlights a broader issue in LA-ICP-MS data handling — the loss of connection between raw data,

results, and available metadata. After measurements and data processing are completed, raw data, results, and metadata often end up scattered across different files or systems. While the results, and in some cases the raw signal data, are typically preserved, most metadata, such as instrument settings or acquisition parameters, are often discarded, except when needed for method development. To address these limitations and to improve on transparency and simplicity of software use, we developed ICP-Base, a free and open-source software featuring an advanced Application User Interface (API) and Graphical User Interface (GUI) designed to maximize user-friendliness, control, and efficiency during data processing of LA-ICP-MS spot analyses. In addition to quantification of solids analyses, it introduces transparent approaches for host-inclusion signal deconvolution for the quantification of fluid or solid inclusion compositions fully enclosed in minerals. A novel algorithm offers the use of multiple external reference materials for parallel and/or sequential quantification procedures.

ICP-Base unifies raw data, processing parameters, results, and LA-ICP-MS metadata within a single centralized database environment. This simplifies long-term instrument monitoring, method development, and retracing past processing decisions. Additionally, integration of the VisModule from MinPlotX (Walters and Gies 2025) enables users to quickly visualize their complete datasets and generate publication-ready figures using self-defined formatting criteria directly within the software environment, without relying on external tools. In this article, we present the software architecture, workflow, and data structure of ICP-Base, and illustrate selected capabilities through case studies on mineral, aqueous fluid and melt inclusion and stalagmite line scan data, showcasing different and novel approaches to quantification, evaluation and data storage.

1. Program design and methodology

ICP-Base is developed in MATLAB® (R2021b) using the MATLAB® App Designer. Stand-alone versions are available for Windows, macOS, and Linux, and can be distributed with or without the MATLAB® Runtime. The Runtime version includes the necessary MATLAB® libraries, allowing ICP-Base to run without an internet connection or a MATLAB® license. This makes it well-suited for installation on laboratory computers without network access. Moreover, as a freely available application, ICP-Base is an excellent resource for students and educators, enabling installation on both personal and university systems. The

software consists of multiple modules, each serving a specific task to guide the user through the data processing (Figure 1).

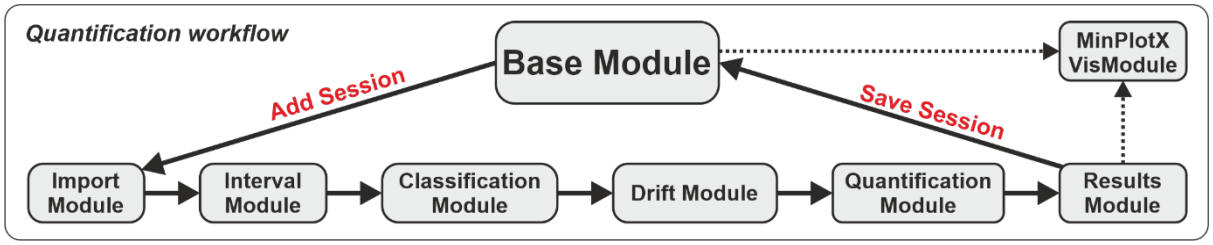

Figure 1: Schematic illustration of the linear element composition quantification workflow. When a new session is added to a project, the user is guided sequentially through the processing modules. Upon completion, all imported signals and metadata, intermediate processing steps, and final results are saved back to the Base (database), from which all processing steps can be revisited. Once the initial workflow is completed, users can freely navigate between the processing modules. The VisModule enables visual evaluation of all data stored in the Base.

1.1. Data structure

The data are organized hierarchically within a database (Base), which can contain multiple projects. Each project can consist of multiple sessions, representing individual measurements or measurement days by a LA-ICP-MS system. Every Session stores the raw data, processed data, and intermediate processing steps (Figure 2). Sessions can also include LA and ICP-MS metadata, given that they are imported. The structure is lightweight and avoids data duplication. All floating-point values are stored using single precision, providing approximately 7 significant decimal digits, which is sufficient since it exceeds LA-ICP-MS analytical data precision. As a result, storing data in ICP-Base requires significantly less memory than saving it in e.g., Microsoft Excel spreadsheets, which uses double precision (15-17 significant digits) by default.

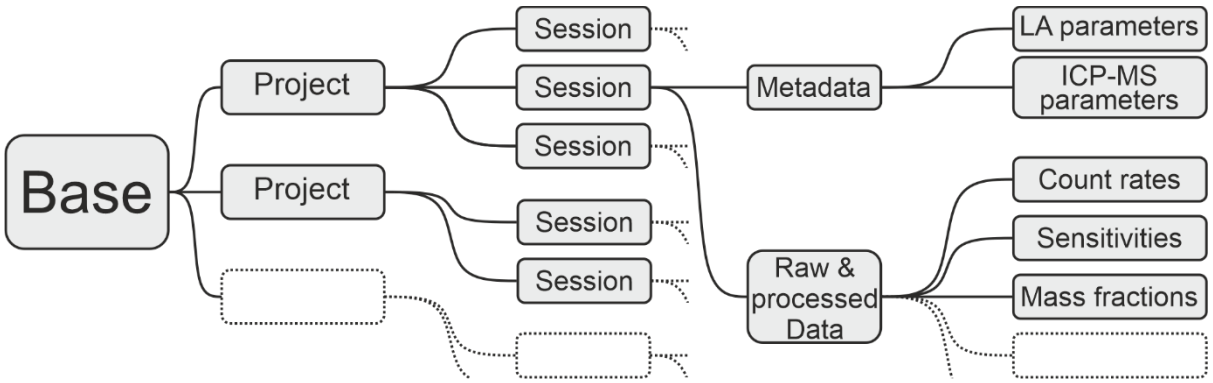

Figure 2: Schematic tree diagram illustrating the hierarchical data organization in ICP-Base. The dashed lines indicate the possible presence of additional projects, sessions and data, illustrating the extendable concept of the data structure hierarchy.

1.2. Application programming interface (API)

ICP-Base provides a versatile API that allows data to be both pushed into and retrieved from its internal data structure. This enables quick access to data of interest, which can then be used directly in scripts or other applications. Furthermore, all data-processing routines can be executed as functions, without relying on the graphical user interface. This makes it possible to perform advanced quantification workflows, for example, running multiple iterations with varying parameters such as the internal standard analyte or mass fraction, entirely within scripts. This capability is particularly useful for method development, implementing Monte Carlo approaches, and organizing datasets in a consistent structure suitable for machine learning applications.

1.3. Modules

1.3.1. Base Module

The Base module serves as the central hub of ICP-Base. It enables users to create and manage multiple projects and sessions. When a new session is added, the linear data processing workflow is initiated (Figure 2, 3). Each session is stored in the Base, providing centralized access to every data processing step (i.e. modules) of all projects and sessions.

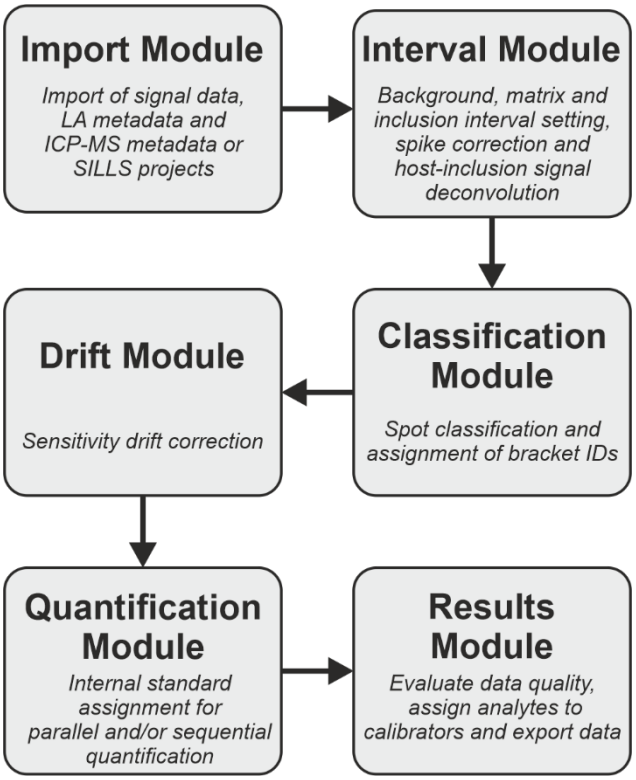

Figure 3: Overview of the functionality of each module for elemental composition quantification.

1.3.2. Import Module

ICP-Base can import three different types of data: (i) Signal data, (ii) LA metadata, and (iii) ICP-MS metadata. For basic data processing only signal data is required. However, for long-term monitoring, it is strongly recommended to import as much metadata as possible. Instrumental metadata are commonly stored for both the LA and ICP-MS measurement sessions.

1.3.2.1. Data type descriptions

Signal data are the raw time-resolved counts-per-second (cps) file(s) holding the data of the ICP-MS measurement. These files are specific to different mass spectrometer brands and can have various file formats. ICP-Base can import two types of signal data: (i) continuous and (ii) single. Continuous signal data consist of one file containing multiple spot analyses, whereas single signal data are organized as individual files, each representing one spot analysis. Additionally, it is also possible to import MAT files previously calculated and saved using the SILLS software (Guillong et al., 2008). In this case, the signal data, the dwell times and the intervals (background, matrix, inclusion) are imported. This makes it quick to evaluate and recalculate former SILLS projects with little effort in ICP-Base.

LA metadata are logbook-style output files generated by the software controlling the laser system when it operates in programmed analysis mode. If the laser was operated manually, a lab-journal-style CSV file based on a provided template can be imported instead. Laser metadata typically include information such as spot names, beam diameters, fluence, repetition rate, gas flows, laser energy, stage positions, and other parameters, depending on what is provided by the laser software.

ICP-MS metadata include file(s) that are output by the ICP-MS systems. These file(s) can hold crucial metadata like the dwell times, which are used for the calculation of the limits of detection (LOD) or machine specific parameters used for monitoring or method development. If the ICP-MS system does not provide such files, a CSV template can be used to manually import the necessary parameters. These machine-specific parameters may include settings related to the plasma (e.g., RF power, plasma gas flows, sampling depth), ion optics (e.g., extraction and focusing lens settings), detector configurations, and other brand- and machine-dependent specifications.

1.3.3. Interval Module

The Interval Module provides a quick and easy way to let the user visually select the data that should be used for further processing by setting background, inclusion and matrix (host) signal intervals, either automatically or manually. Automatically set signal intervals can be easily checked and manually modified if needed. The module features a spike removal function that applies a moving-window Grubbs' test (Grubbs, 1969) at a 1% significance level to detect and eliminate outliers.

Signal visualization in the Interval Module is fully customizable through user-defined CSV plot style files. Each analyte's appearance, such as marker color, size, and shape, as well as line color, width, and style, can be individually adjusted to suit the user preference. Users can also visualize intensity ratios by specifying a numerator and denominator in the plot style file, allowing element ratios to be plotted on a per-sweep basis.

In addition to the default interval settings for mineral quantification, this module includes the matrix-only tracer algorithm for host-inclusion deconvolution, making the process more transparent and allowing users to visually assess the quality of the results.

1.3.3.1. Transient signal description and interval definitions

The obtained transient signal acquired by ablation of a given sample is best described by using the equations and nomenclature presented in Guillong et al. (2008):

$$I_{\mathrm{i}}^{\mathrm{SIG1}} = I_{\mathrm{i}}^{\mathrm{BG}} \quad (1)$$

$$I_{\mathrm{i}}^{\mathrm{SIG2}} = I_{\mathrm{i}}^{\mathrm{BG}} + I_{\mathrm{i}}^{\mathrm{HOST(SIG2)}} \quad (2)$$

$$I_{\mathrm{i}}^{\mathrm{SIG3}} = I_{\mathrm{i}}^{\mathrm{BG}} + I_{\mathrm{i}}^{\mathrm{HOST(SIG3)}} + I_{\mathrm{i}}^{\mathrm{INCL}} \quad (3)$$

where *I* refers to the mean count rate (in cps) of an analyte i in the given signal interval (BG = background and SIG = sample signal) and HOST refers to host mineral and INCL refers to the inclusion-host mixed signal interval (Figure 4).

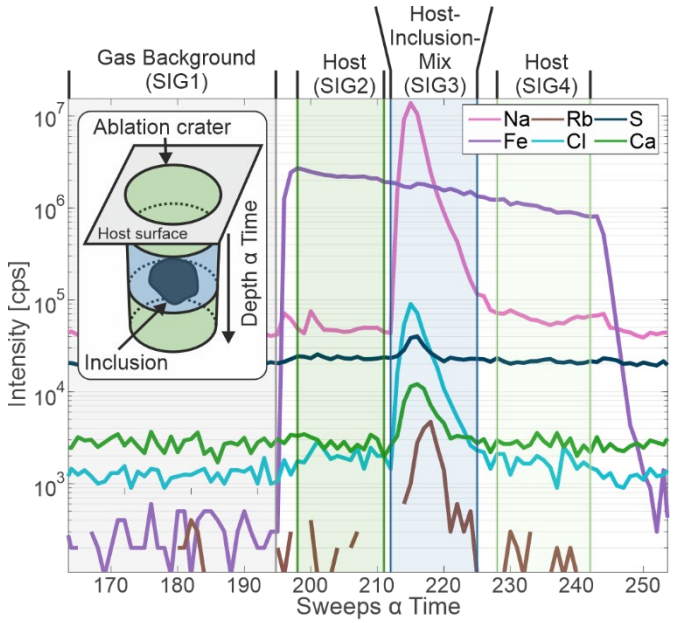

Figure 4: Examples of transient analyte count rates acquired by ablation of a fluid inclusion relic in olivine from a Chl-Harzburgite (Cerro del Almirez, Spain). The inset illustrates the principle of LA-ICP-MS analysis of fully enclosed inclusions. The colored segments in the inset correspond to the signal segments. The transient signal consists of four segments: (i) The gas background (SIG1). (ii) The signal of the host ablated before reaching the inclusion (SIG2). (iii) The host-inclusion-mix signal where the host and the inclusion are ablated simultaneously (SIG3). (iv) Signal of the host below the inclusion after it was fully ablated (SIG4).

The calculations for SIG4 are performed analogously to those for SIG2 and are not presented further. Net analyte signal intensities are obtained by subtracting I_i^{BG}:

$$I_{\mathrm{i}}^{\mathrm{HOST(SIG2)}} = I_{\mathrm{i}}^{\mathrm{SIG2}} - I_{\mathrm{i}}^{\mathrm{BG}} \quad (4)$$

$$I_{\mathrm{i}}^{\mathrm{MIX}} = I_{\mathrm{i}}^{\mathrm{SIG3}} - I_{\mathrm{i}}^{\mathrm{BG}} = I_{\mathrm{i}}^{\mathrm{HOST(SIG3)}} + I_{\mathrm{i}}^{\mathrm{INCL}} \quad (5)$$

1.3.3.2. Matrix-only tracer algorithm

This approach, first implemented in SILLS (Guillong et al., 2008), makes use of an analyte chosen as a matrix-only tracer (t) that is significantly present in the host mineral but not in the inclusion. With the matrix-only tracer, an intensity ratio R of the intensities in the host mineral (*Eq.6*) and host-inclusion-mix (*Eq.7*) can be defined and is expressed as:

$$R = \frac{I_{\mathrm{i}}^{\mathrm{HOST(SIG3)}}}{I_{\mathrm{i}}^{\mathrm{HOST(SIG2)}}} \quad (6)$$

Since the definition of a matrix-only tracer is, that it has a negligible intensity in the inclusion, it can be stated that $I_{\mathrm{t}}^{\mathrm{INCL}} = 0$. It follows that $I_{\mathrm{t}}^{\mathrm{HOST(SIG3)}} = I_{\mathrm{t}}^{\mathrm{MIX}}$ and the Eq. 6 simplifies to:

$$R = \frac{I_{\mathrm{t}}^{\mathrm{HOST(SIG3)}}}{I_{\mathrm{t}}^{\mathrm{HOST(SIG2)}}} = \frac{I_{\mathrm{t}}^{\mathrm{MIX}}}{I_{\mathrm{t}}^{\mathrm{HOST(SIG2)}}} \quad (7)$$

Since both, $I_{\mathrm{t}}^{\mathrm{MIX}}$ and $I_{\mathrm{t}}^{\mathrm{HOST(SIG2)}}$ are known, the R can be calculated once and used to deconvolve all analyte intensities of the host-inclusion-mix to the inclusion contributions $I_{\mathrm{i}}^{\mathrm{INCL}}$ within the same analysis. To solve for the intensities of the host contribution to the host-inclusion-mix Eq. 6 is rearranged and expressed as:

$$I_{\mathrm{i}}^{\mathrm{HOST(SIG3)}} = R \times I_{\mathrm{i}}^{\mathrm{HOST(SIG2)}} \quad (8)$$

By subsequent substitution for $I_{\mathrm{i}}^{\mathrm{HOST(SIG3)}}$ in Eq. 5 the equation is rewritten as:

$$I_{\mathrm{i}}^{\mathrm{INCL}} = I_{\mathrm{i}}^{\mathrm{MIX}} - I_{\mathrm{i}}^{\mathrm{HOST(SIG3)}} = I_{\mathrm{i}}^{\mathrm{MIX}} - R \times I_{\mathrm{i}}^{\mathrm{HOST(SIG2)}} \quad (9)$$

The host-inclusion-mix is thus resolved into its pure inclusion ($I_{\mathrm{i}}^{\mathrm{INCL}}$) and host ($I_{\mathrm{i}}^{\mathrm{SIG3(Host)}}$) intensity contributions.

1.3.4. Classification Module

The Classification Module allows the user to define the role of each measurement spot as unknown (UNK), calibrator (CAL), quality control reference material (QCRM), or interference correction material (ICM). An unknown is any mineral or inclusion whose composition is to be quantified. The CAL (calibration standard) provides analyte sensitivity calibration for quantifying the measurements of the

unknown. Note that multiple CAL's can be specified, to be employed later for quantification. A QCRM is treated identically to an unknown during data processing but has a known composition and is used for quality control. An ICM is a material which can be used for interference correction.

If CALs are measured under different analytical conditions, such as varying beam size or laser repetition rate, they need to be treated separately to avoid incorrect drift correction, since changes in these parameters may produce variations in analyte sensitivity ratios related to the variable laser aerosol load in the plasma. To manage this, a bracket ID can be assigned to each CAL spot (Figure 5). CALs from the same reference material and bracket ID are grouped together, and such CAL-bracket ID groups are treated independently during subsequent data processing.

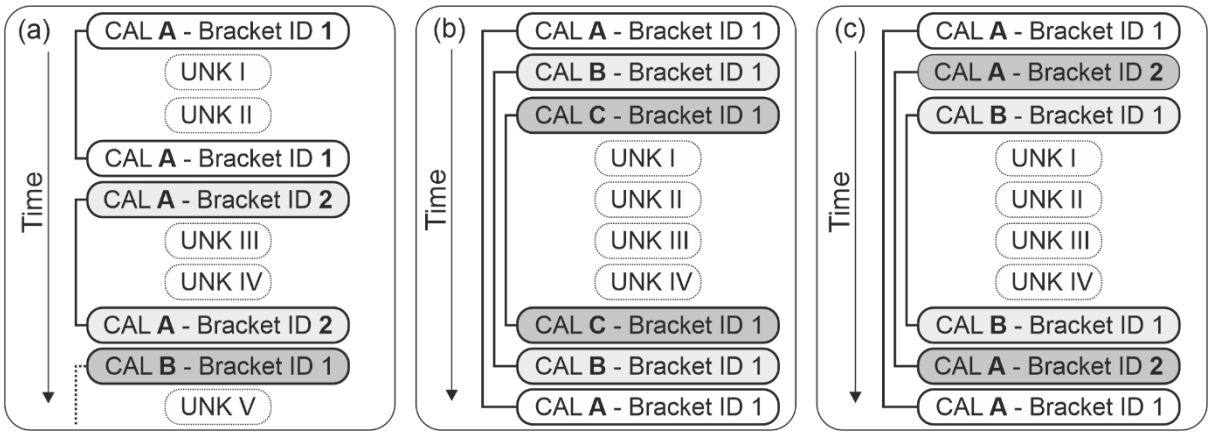

Figure 5: Schematic illustration of possible calibration standard (CAL) – unknown (UNK) bracket layouts. (a) Example in which the same CAL A is used with different bracket IDs to reflect varying analytical conditions. UNK I and UNK II were measured with a 20 µm beam diameter while UNK III and UNK IV were measured with an 80 µm beam diameter. The analysis of calibration standard CAL A was thus beam-diameter-matched to the respective UNK. Note that such a separation can be done for any reason and is not bound to beam diameter. A different CAL ("B") may be used for subsequent unknowns. (b) Example of four unknowns that are bracketed by three CALs (A, B and C) of the same bracket ID. This bracketing layout is used in figure 6. Note that bracket IDs are not needed to separate different CALs (A, B and C) because the CALs are uniquely defined by their names. Additional or alternative brackets may follow, as shown in (a). (c) Example bracketing layout in which CAL A is assigned two bracket IDs, while an additional CAL B is also used to quantify the same unknowns. Such a configuration may be applied, for example, when CAL A is measured using different analytical conditions (analogous to example (a)) to evaluate their influence on the quantification of UNK I–IV.

1.3.5. Drift Module

The Drift Module calculates and visualizes the drift in analyte sensitivities during a given measurement session. Analyte sensitivities for all calibrators are calculated individually based on the analyte intensities within the intervals defined in the Interval Module and the reference materials specified in the Classification Module. Consecutive CAL spots belonging to the same CAL–bracket ID group, and separated by non-CAL spots (including UNK and optionally QCRM and IHRM), define the start and end points of a bracket. The sensitivities of these CAL spots are averaged to obtain representative values for each bracket position i.e. a bracket start and end. The acquisition times of all spots are then converted into integer time points, reflecting their relative positions within the measurement sequence and allowing for more efficient data handling. A linear regression is subsequently fitted between the averaged sensitivities of each analyte and their corresponding central integer time points, extending from one averaged set CAL to the next. All remaining non-CAL spots are then corrected for sensitivity drift by interpolating their values along this fitted line, thus correcting all measurement intensities for true-time instrumental drift throughout the measurement session.

1.3.6. Quantification Module

For accurate quantification of any LA-ICP-MS data, internal standardization is required to convert apparent analyte sensitivities as determined on the CAL into true analyte sensitivities to be applied to each measurement spot. ICP-Base offers two types of internal standardization approaches: (i) Use of any known analyte mass fraction in μg g^{-1}. (ii) a normalization to a given mass fraction sum of element oxides (Total Oxides). In the Quantification Module, users can assign the type of internal standardization to each spot individually for every CAL–bracket ID pair. Both the host and the inclusion of a spot can be quantified simultaneously, each using its own dedicated internal standardization criterion. All quantification strategies implemented in ICP-Base adhere to established and proven LA-ICP-MS quantification principles (Guillong et al., 2008).

1.3.6.1. Conventional quantification procedure

LA-ICP-MS quantification requires internal standardization, here illustrated using an analyte with known mass fraction (is). Using the drift-corrected sensitivities $S_{\mathrm{i}}^{\mathrm{DC}}$, analyte mass fractions are obtained from:

$$C_{\mathrm{i}} = \frac{I_{\mathrm{i}}}{I_{\mathrm{is}}} \times \frac{C_{\mathrm{is}}}{S_{\mathrm{i}}} \tag{10}$$

Where C_{i} and C_{is} are the mass fractions C of analyte i and the internal standard is in µg g^{-1}, respectively. For the host mineral (SIG2), sensitivities are normalized to the internal-standard analyte in the host (is0):

$$S_{\mathrm{i}}^{\mathrm{HOST(SIG2)}} = \frac{S_{\mathrm{i}}^{\mathrm{DC}}}{S_{\mathrm{is0}}^{\mathrm{DC}}} \tag{11}$$

Once established, the mass fractions of all analytes in the $\mathrm{HOST(SIG2)}$ interval can be calculated according to Eq. 10 as:

$$C_{\mathrm{i}}^{\mathrm{HOST(SIG2)}} = \frac{I_{\mathrm{i}}^{\mathrm{HOST(SIG2)}}}{I_{\mathrm{is0}}^{\mathrm{HOST(SIG2)}}} \times \frac{C_{\mathrm{is0}}^{\mathrm{HOST(SIG2)}}}{S_{\mathrm{i}}^{\mathrm{HOST(SIG2)}}} \tag{12}$$

1.3.6.2. Inclusion quantification for pure inclusion intensities

The pure inclusion intensities, calculated using a Matrix-only tracer in the Interval Module, are now used to perform inclusion quantification. Analogous to Eq. 11, the analytical sensitivities of the analytes in the sample are first normalized to the analytical sensitivity of one analyte with a known mass fraction chosen as an internal standard $\mathrm{is1}$.

$$S_{\mathrm{i}}^{\mathrm{MIX}} = \frac{S_{\mathrm{i}}^{\mathrm{DC}}}{S_{\mathrm{is1}}^{\mathrm{DC}}} \tag{13}$$

Next, the mass fraction ratios $a_{\mathrm{i/is1}}^{\mathrm{INCL}}$ are calculated for every analyte in the measurement.

$$a_{\mathrm{i/is1}}^{\mathrm{INCL}} = \frac{C_{\mathrm{i}}^{\mathrm{INCL}}}{C_{\mathrm{is1}}^{\mathrm{INCL}}} = \frac{I_{\mathrm{i}}^{\mathrm{INCL}}}{I_{\mathrm{is1}}^{\mathrm{INCL}}} \times \frac{1}{S_{\mathrm{i}}^{\mathrm{MIX}}} \tag{14}$$

Finally, the mass fractions of the analytes in the inclusion are calculated.

$$C_{\mathrm{i}}^{\mathrm{INCL}} = a_{\mathrm{i/is1}}^{\mathrm{INCL}} \times C_{\mathrm{is1}}^{\mathrm{INCL}} \tag{15}$$

1.3.6.3. Two internal standard inclusion quantification

Inclusion quantification can also be achieved by the use of two internal standards, i.e. analytes with known mass fractions in the inclusion referred to as $\mathrm{is1}$ and $\mathrm{is2}$ (Guillong et al., 2008). They are necessary to determine the mixing ratio x, defined as the mass (m) ratio of the inclusion in the total ablated host-inclusion-mix (Halter et al., 2002). It can be expressed as:

$$x = \frac{m^{\mathrm{INCL}}}{m^{\mathrm{MIX}}} = \frac{C_{\mathrm{i}}^{\mathrm{HOST(SIG2)}} - C_{\mathrm{i}}^{\mathrm{MIX}}}{C_{\mathrm{i}}^{\mathrm{HOST(SIG2)}} - C_{\mathrm{i}}^{\mathrm{INCL}}} = \frac{C_{\mathrm{is}}^{\mathrm{HOST(SIG2)}} - C_{\mathrm{is}}^{\mathrm{MIX}}}{C_{\mathrm{is}}^{\mathrm{HOST(SIG2)}} - C_{\mathrm{is}}^{\mathrm{INCL}}} \tag{16}$$

To determine x, we first have to normalize the sensitivities of the analytes in the sample to the sensitivity of is2, analogous to Eq. 11.

$$S_{\mathrm{i}}^{\mathrm{MIX}} = \frac{S_{\mathrm{i}}^{\mathrm{DC}}}{S_{\mathrm{is2}}^{\mathrm{DC}}} \tag{17}$$

Next, Eq. 10 is rearranged to express the mass fraction ratios $a_{\mathrm{i/is}}^{\mathrm{SAMP}}$ of all analytes in the sample relative to the mass fraction of the internal standard:

$$a_{\mathrm{i/is}}^{\mathrm{SAMP}} = \frac{C_{\mathrm{i}}^{\mathrm{SAMP}}}{C_{\mathrm{is}}^{\mathrm{SAMP}}} = \frac{I_{\mathrm{i}}^{\mathrm{SAMP}}}{I_{\mathrm{is}}^{\mathrm{SAMP}}} \times \frac{1}{S_{\mathrm{i}}^{\mathrm{DC}}} \tag{18}$$

This equation can further be specified to express the mass fraction ratio $a_{\mathrm{is1/is2}}^{\mathrm{MIX}}$ of both internal standards in the host-inclusion-mix:

$$a_{\mathrm{is1/is2}}^{\mathrm{MIX}} = \frac{C_{\mathrm{is1}}^{\mathrm{MIX}}}{C_{\mathrm{is2}}^{\mathrm{MIX}}} = \frac{I_{\mathrm{is1}}^{\mathrm{MIX}}}{I_{\mathrm{is2}}^{\mathrm{MIX}}} \times \frac{1}{S_{\mathrm{is1}}^{\mathrm{MIX}}} \tag{19}$$

Since all variables in this equation are known, $a_{\mathrm{is1/is2}}^{\mathrm{MIX}}$ can be calculated. Rearranging Eq. 16 twice to express $C_{\mathrm{is1}}^{\mathrm{MIX}}$ and $C_{\mathrm{is2}}^{\mathrm{MIX}}$ and subsequently substituting these variables in Eq. 19 makes it possible to re-express $a_{\mathrm{is1/is2}}^{\mathrm{MIX}}$ as:

$$C_{\mathrm{is1}}^{\mathrm{MIX}} = (1 - x) \times C_{\mathrm{is1}}^{\mathrm{HOST(SIG2)}} + x \times C_{\mathrm{is1}}^{\mathrm{INCL}} \tag{20}$$

$$C_{\mathrm{is2}}^{\mathrm{MIX}} = (1 - x) \times C_{\mathrm{is2}}^{\mathrm{HOST(SIG2)}} + x \times C_{\mathrm{is2}}^{\mathrm{INCL}} \tag{21}$$

$$a_{\mathrm{is1/is2}}^{\mathrm{MIX}} = \frac{C_{\mathrm{is1}}^{\mathrm{MIX}}}{C_{\mathrm{is2}}^{\mathrm{MIX}}} = \frac{(1 - x) \times C_{\mathrm{is1}}^{\mathrm{HOST(SIG2)}} + x \times C_{\mathrm{is1}}^{\mathrm{INCL}}}{(1 - x) \times C_{\mathrm{is2}}^{\mathrm{HOST(SIG2)}} + x \times C_{\mathrm{is2}}^{\mathrm{INCL}}} \tag{22}$$

Finally, Eq. 22 is rearranged to solve for the mixing ratio x, which is then expressed as a function of mass fraction ratio $a_{\mathrm{is1/is2}}^{\mathrm{MIX}}$ and of known mass fractions of the internal standards in the inclusion and the host mineral:

$$x = \frac{C_{\mathrm{is1}}^{\mathrm{HOST(SIG2)}} - a_{\mathrm{is1/is2}}^{\mathrm{MIX}} \times C_{\mathrm{is2}}^{\mathrm{HOST(SIG2)}}}{C_{\mathrm{is1}}^{\mathrm{HOST(SIG2)}} - C_{\mathrm{is1}}^{\mathrm{INCL}} - a_{\mathrm{is1/is2}}^{\mathrm{MIX}} \times C_{\mathrm{is2}}^{\mathrm{HOST(SIG2)}} + a_{\mathrm{is1/is2}}^{\mathrm{MIX}} \times C_{\mathrm{is2}}^{\mathrm{INCL}}} \tag{23}$$

Once *x* is defined, the mass fraction of internal standard is2 in the host-inclusion-mix $C_{\mathrm{is2}}^{\mathrm{MIX}}$ is calculated using Eq. 21. With Eq. 10, the mass fractions of all analytes in the host-inclusion-mix are calculated:

$$C_{\mathrm{i}}^{\mathrm{MIX}} = \frac{I_{\mathrm{i}}^{\mathrm{MIX}}}{I_{\mathrm{is2}}^{\mathrm{MIX}}} \times \frac{C_{\mathrm{is2}}^{\mathrm{MIX}}}{S_{\mathrm{i}}^{\mathrm{MIX}}} \tag{24}$$

Finally, by rearranging Eq. 16 to solve for $C_{\mathrm{i}}^{\mathrm{INCL}}$, the mass fractions of all analytes in the pure inclusion are quantified:

$$C_{\mathrm{i}}^{\mathrm{INCL}} = \left(\frac{1}{x}\right) \times C_{\mathrm{i}}^{\mathrm{MIX}} - \left(\frac{1-x}{x}\right) \times C_{\mathrm{i}}^{\mathrm{HOST(SIG2)}} \tag{25}$$

1.3.6.4. Parallel quantification

When multiple CALs and bracket IDs are used, ICP-Base performs separate sensitivity calculations and corrections for each unique CAL–bracket ID pair. As a result, every non-CAL spot can be quantified multiple times, once for each pair (Figure 5). This allows for direct comparison of results derived from different CALs and measurement conditions. In essence, the software generates multiple quantification strands that run in parallel (Figure 6).

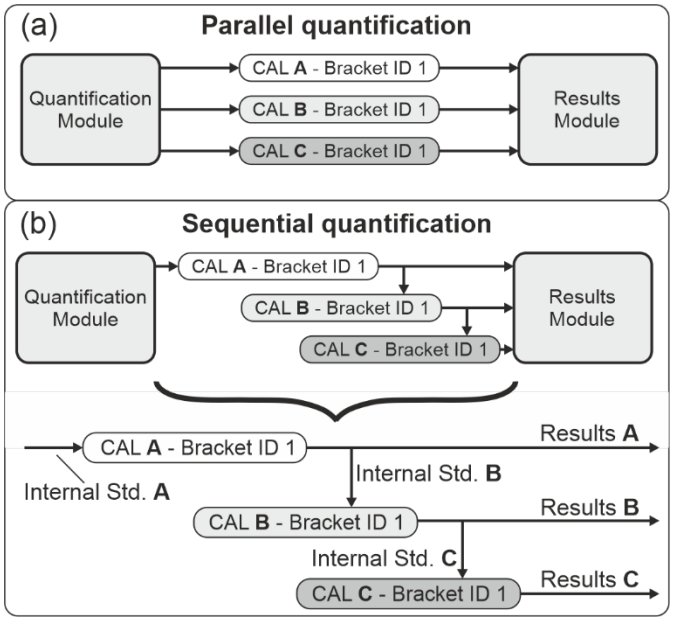

Figure 6: Schematic illustration of parallel and sequential quantification using three calibration standards (CALs A, B, and C). The bracketing layout shown in Figure 5b is applied; consequently, all brackets contain the same unknowns (UNK) to be quantified. Fields labeled, for example, "CAL A – Bracket ID 1" represent brackets containing UNK spots used for quantification (see Figure 5). (a) Parallel quantification using three CALs (A, B and C). For each bracket (e.g., CAL A – Bracket ID 1), all UNKs are assigned an internal standard independently and quantified in parallel. (b) Sequential quantification is performed iteratively using CALs A, B, and C. In the first step, UNKs are assigned Internal Standard A and quantified using CAL A – Bracket ID 1. Based on the resulting outputs (Results A), the same UNKs are

subsequently reassigned Internal Standard B and quantified using CAL B – Bracket ID 1. This procedure is then repeated for CAL C – Bracket ID 1. In principle, this sequential approach can be extended to an arbitrary number of successive quantification steps. Importantly, Internal Standards B and C can be derived directly from Results A.

1.3.6.5. Sequential quantification

While ICP-Base already provides considerable flexibility via parallel quantification, sequential quantification allows for further enhanced control and versatility. Instead of processing each CAL–bracket ID pair in parallel, the software can apply them in sequence, allowing results from one quantification strand to be used by subsequent quantification strands (Figure 6).

Sequential quantification is especially useful when the selected internal standard analyte is present or well-characterized in only one of the calibrators. In such cases, the user can choose to first quantify the samples using the reference material that contains the desired internal standard analyte. The results from this initial quantification, specifically the mass fraction of one user-defined analyte, is then used as internal standard for subsequent quantification with another reference material. This creates a stepwise process in which each quantification step builds on the results of the previous one(s). It allows the user to link multiple calibrators in a sequence, ensuring that standards missing certain elements can still be used effectively.

1.3.7. Results Module

In the Results Module, users can evaluate and export quantification results for each CAL–Bracket ID pair. Mass fractions (µg g^{-1}) can be viewed either with or without LOD filtering (using the formulation of Pettke et al., 2012) and converted to element-oxide equivalents (% m/m) if needed. The module also provides access to sensitivities, the LODs, and background-corrected intensity data for both matrix and inclusion intervals for all spots. For all spots classified as QCRM, the module provides a plot showing the ratio of quantified results to the reference composition defined for each reference material. This visualization offers an immediate assessment of how accurately the QCRMs were reproduced during the measurement session. If multiple CALs were used for quantification, analytes can be individually assigned to a respective CAL, and the resulting output table is generated accordingly.

2. Application examples

To demonstrate the usability of ICP-Base across different scientific applications, data from multiple analytical setups, including varied bracket layouts, sequential and parallel quantification, and both mineral and inclusion analysis is processed. For the inclusions both, the deconvolution and quantification via two internal standards and matrix-only tracer is showcased. A petrological application is presented by processing mineral data from ultramafic rocks, including the use of secondary and in-house reference materials analyzed during these measurements for short- and long-term monitoring. Quartz-hosted fluid inclusions highlight applications in fluid inclusion research, while melt inclusions in various host minerals demonstrate use in magmatic and volcanic studies. For paleoclimate research, processing of a stalagmite line scan using a moving average is presented. All data processing, evaluation, and visualization are performed entirely within the ICP-Base environment, enabling an efficient workflow without switching between multiple software. The quantification results of all examples are visualized using the integrated VisModule (Walters and Gies, 2025), which is accessed directly through the Base Module.

2.1. Quantification, evaluation and visualization within the ICP-Base software environment

To illustrate the quantification of mineral analyses, the evaluation of secondary and in-house reference materials, and the visualization of results from multiple measurement sessions stored within the same base, three LA-ICP-MS datasets, acquired over the course of ~2 years at the University of Bern, are processed. By integrating these datasets within a centralized data structure, the advantages of consistent data storage over a long time are demonstrated.

The data comprise mineral analyses of Chl-harzburgite from Cerro del Almirez (Sierra Nevada, Spain) (Figure 7a), Val Cama (Alps, Switzerland), and Gana Rossa (Alps, Switzerland). The geochemistry of these metaperidotites records a complex history of magmatic depletion and re-fertilization, followed by oceanic hydration and subduction metamorphic dehydration. A comprehensive description of the mineralogy, sample characteristics, and geological setting of Gana Rossa is provided in Stucki et al., (2001) and Thurnherr (2025). The samples from Cerro del Almirez are documented and discussed in Bretscher et al. (2018), Pettke and Bretscher (2022), and Vieira Duarte et al. (2021). Metaperidotites from

Val Cama are described in Vieira Duarte et al. (2023). Documentation of the analytical conditions employed can be found in the supplementary material (Table S1). SRM 612 was analyzed as a quality control reference material during the measurement session of the Gana Rossa samples, and the resulting quantification is evaluated through comparison with published reference values. In addition, the in-house San Carlos olivine reference material W2-Ol was measured in all sessions, and its results are compared to assess long-term reproducibility and inter-session consistency.

Multiple brackets of GSD-1G used as CAL were employed in all analytical sessions. Within each session, all GSD-1G spots were measured under identical analytical conditions; therefore, no subdivision of the CALs by bracket ID was applied. Nominally anhydrous olivine and orthopyroxene analyses were normalized to 100 wt% total oxides for internal standardization, whereas volatile-bearing chlorite was normalized to 87.9 wt% total oxides (i.e., 100 wt% - stoichiometric H_2O). SRM 612 was normalized to 100 wt% total oxides.

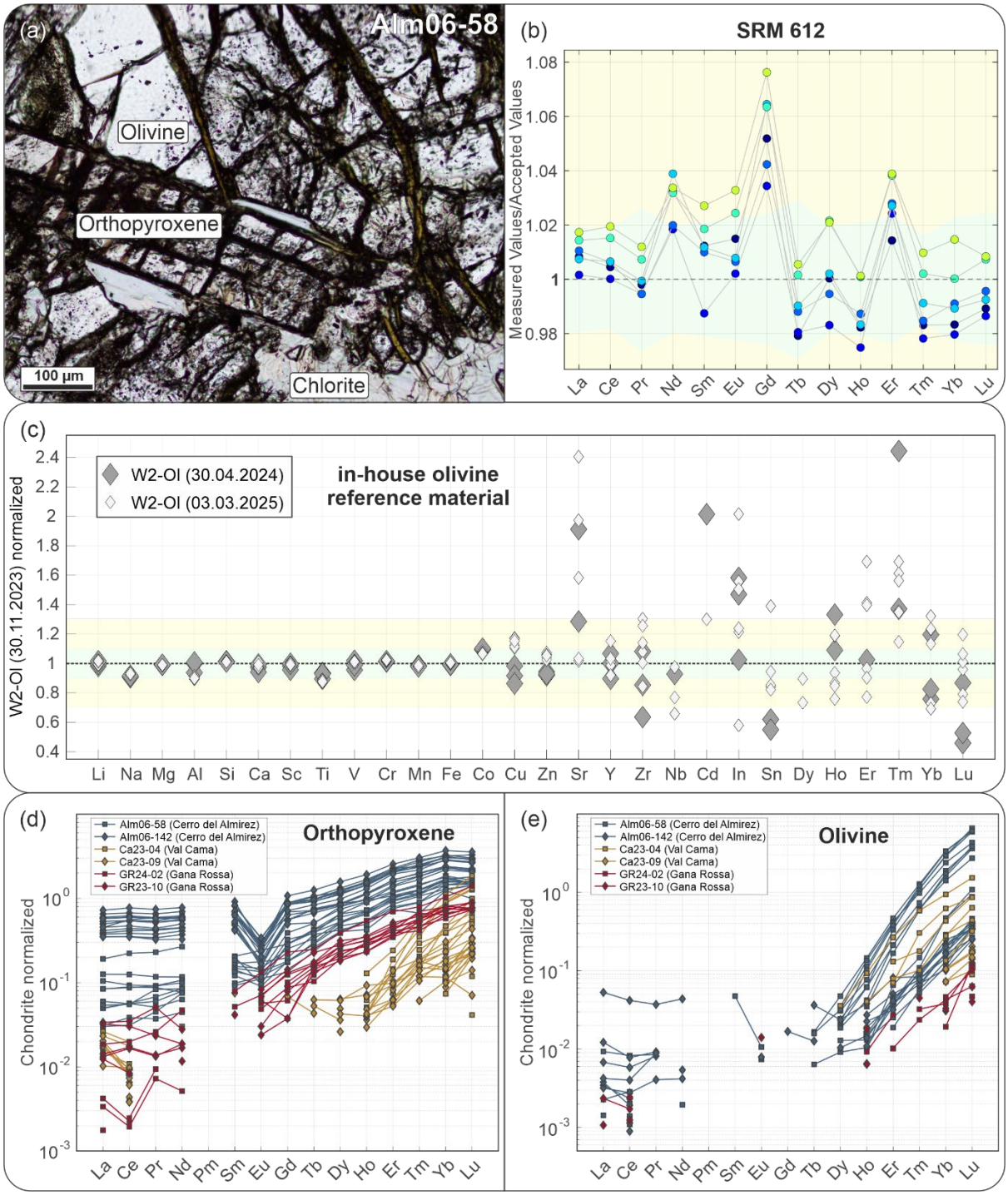

Figure 7: (a) Thin-section photograph of a granular Chl-harzburgite sample from Cerro del Almirez. (b) REE mass fractions measured in the quality control reference material SRM 612, shown as ratios to the reference values. The light green field indicates the uncertainty of the reference values; the light yellow field represents the reference uncertainty ±10%, while symbol colors follow a Jet colour scale to indicate the relative timing of analyses (black marking the earliest measurements and lime the latest) to visualize potential residual drift. (c) Mass fraction ratios of selected elements measured in the in-house reference material W2-Ol over a period of ~2 years. Data acquired on

30.04.2024 and 03.03.2025 are normalized to those obtained on 30.11.2023 to evaluate reproducibility and identify potential temporal trends. The light green field marks ±10% deviation, and the light yellow field marks ±20%. The large variation in measurement data for elements heavier than Sr result from their ultratrace mass fractions, commonly below 100 ng g^{-1}. (d) Chondrite-normalized REE plot for orthopyroxene. Chondrite values are from McDonough and Sun 1995 (e) Chondrite-normalized REE plot for olivine. Results below the respective detection limits are omitted in all plots.

SRM 612 was systematically analyzed as QCRM once per bracket during the Gana Rossa measurement session, with analyses spaced approximately 20–30 minutes apart. Using a built-in function of the Results Module, the quantified REE mass fractions were ratioed to their reference values to evaluate analytical accuracy (Figure 7b). For most measurements, the REEs were reproduced within the uncertainty of their reference values. A notable exception is Gd, which was consistently quantified above the reference value and its associated uncertainty, the deviation remained still within 5% of the reference mass fraction, however, and is thus not severe. Although the data were corrected for instrumental sensitivity drift, a minor residual drift in the quantified results can be observed over the course of the session. This trend is particularly evident for Tb, Ho, Tm, Yb, and Lu, which were quantified below their reference values in the first four analyses but above the reference values in the final two measurements.

The in-house San Carlos reference material W2-Ol was analyzed in all three measurement sessions (Cerro del Almirez: 30.11.2023, Val Cama: 30.04.2024, Gana Rossa: 03.03.2025) to monitor long-term reproducibility. Because each session includes quantified results and metadata, and all data are stored within the centralized ICP-Base structure, comparisons across sessions can be performed directly without additional reorganization. Major olivine elements (Mg, Fe, Si) were reproduced within ±2% relative to 2023, while non-major elements (Li, Na, Al, Ca, Sc, Ti, V, Cr, Mn, Co, Zn) generally agreed within ±10% (Figure 7c). Most other monitored low-abundance elements show larger variability, with maximum deviations of +140% (Tm, 2024) and −35% (Lu, 2024), which is typical for low mass fraction elements near the respective analytical limits of detection where measurement uncertainties along with scatter in data increase prominently. Systematic temporal trends were observed for Cu and Zn (lower in 2024, higher in 2025) and for Al, Ti, and Co (lower in 2025). Overall, the results demonstrate good reproducibility for major and minor elements, while low-abundance trace elements show the expected elevated variability. If LA and ICP-MS metadata (e.g., spot diameter, laser fluence, gas flows) are imported, these system-

specific parameters can also be used for further evaluation directly within the software environment. Additionally, long-term monitoring could also be carried out using different materials such as SRM 612 and be based on raw cps data or sensitivities to monitor instrument performance.

The quantified REE mass fractions for orthopyroxene and olivine from the different localities were compared to chondritic values. Because all spots are tagged with metadata (sample, mineral type, locality) and stored in the centralized ICP-Base database, such comparisons can be performed directly within the software. Orthopyroxene from two samples per locality shows a consistent chondrite-normalized REE pattern (Figure 7d). Cerro del Almirez data has the highest REE mass fractions, followed by Gana Rossa and Val Cama, with all localities showing enrichment in HREEs relative to LREEs. HREEs exceed chondritic values in all Cerro del Almirez analyses, one Gana Rossa analysis, and four Val Cama analyses, while most LREE are below chondrite. Olivine shows a similar REE pattern, with HREEs enriched relative to LREEs (Figure 7e). Cerro del Almirez data again has the highest REE mass fractions. Within Cerro del Almirez data set, olivine from the granular-textured sample Alm06-58 is displays conspicuously higher REE contents than olivine from sample Alm06-142. Data for olivine from Gana Rossa and Val Cama is plot generally below those for Almirez, except for a single slightly enriched analysis from sample Ca23-04 (Val Cama).

2.2. Sequential quantification of fluid inclusions

Data from fluid inclusions (FI) in cleft-quartz collected at Spittellamm (Aar Massif, Central European Alps; Arnold, 2022), are used to illustrate the importance of transparent host–inclusion signal deconvolution using a matrix-only tracer. Chlorine calculated from wt% NaCl equivalent as determined by microthermomentry is applied as the internal standard, and two external standards are used sequentially to quantify the paleo-fluid composition.

Alpine fissures are long-lived, fluid-filled cavities that form at mid-crustal depths and record several million years of progressive exhumation. Fluid–rock interaction along fissure walls leads to mineral dissolution and the growth of diverse mineral assemblages, with quartz being the most abundant and best-suited host for FI. Quartz-hosted FI preserve direct information on paleo-fluid composition and salinity, allowing for reconstruction of fluid evolution with progressive crystal growth. Twenty-seven FI in

quartz were analyzed in sample TA-F3 (Figure 8a). The LA-ICP-MS measurement conditions are outlined in Arnold (2022).

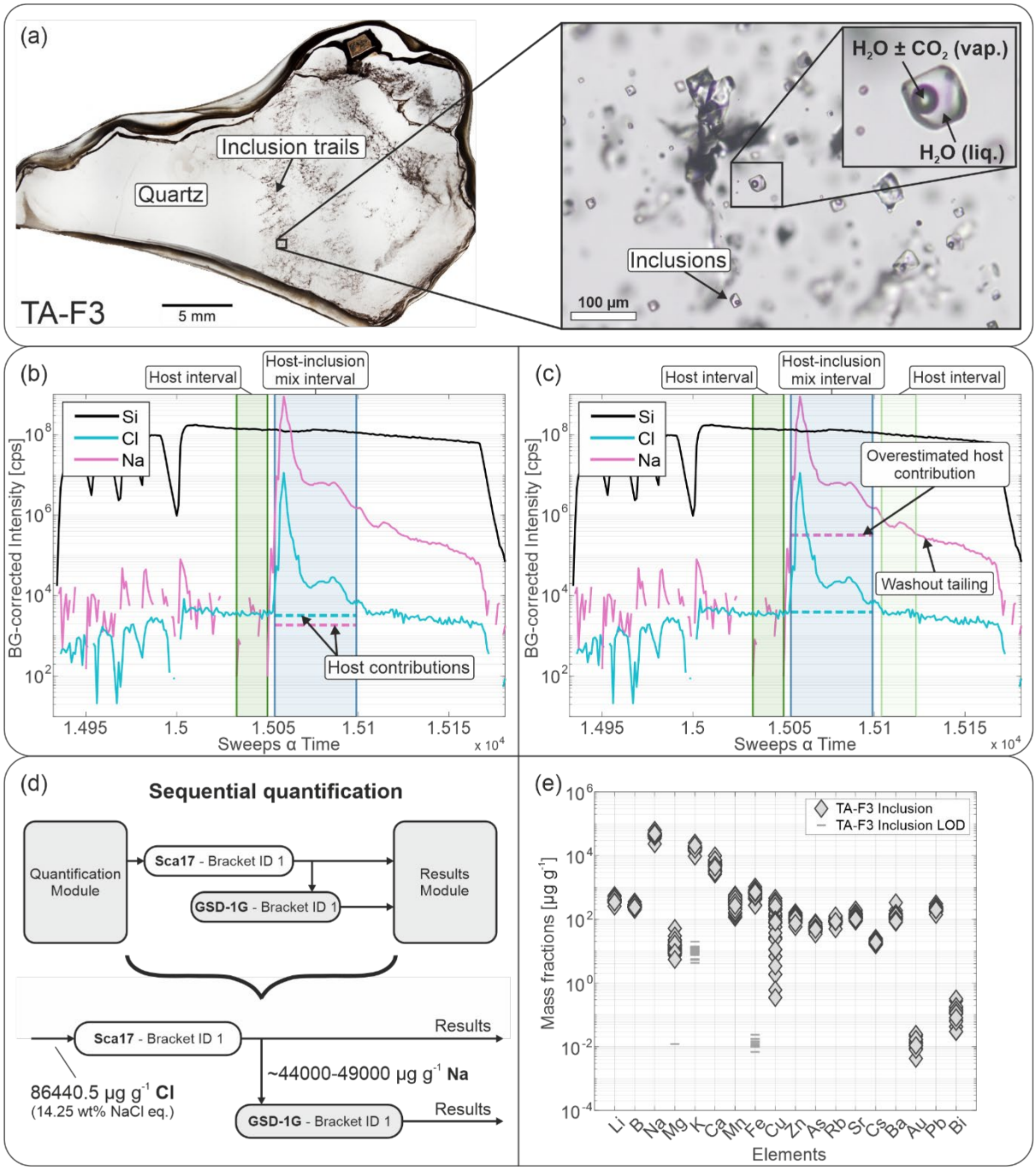

Figure 8: (a) Photograph of cleft quartz thick section TA-F3. Inset shows a close-up view of fluid inclusions fully enclosed within the host quartz. (b) Background-corrected intensity signal plotted over time, with one host interval defined prior to the host–inclusion–mix interval. Horizontal dashed lines indicate the calculated host contributions to the mixed signal for the respective elements. (c) Same as (b), however, with two host intervals defined before and after the host–inclusion–mix interval. The Na host contribution is overestimated in this case due to washout tailing of

the Na signal and thus incorrect. This example is included deliberately to illustrate the importance of correct interval selection. (d) Schematic illustration of the sequential quantification procedure (compare Figure 6). Note that the Na mass fractions (~44000-49000 µg g^{-1}) are calculated individually for each inclusion analysis based on the use of a constant Cl mass fraction for quantification step 1. (e) Mass fractions of selected elements measured in fluid inclusions from sample TA-F3 quantified using GSD-1G as CAL. Limits of detection (LODs) are indicated for elements with mass fractions below the detection limit.

One host interval was set per spot, and Si was used as the matrix-only tracer for host-inclusion signal deconvolution. By plotting the background-corrected signal intensity data, the host contribution to the host-inclusion mixed signal is made visible and can be used to assess the deconvolution quality (Figure 8b). The transient signals show that some analytes (Na in Figure 8b) have a washout time that is longer than the total ablation duration (i.e. inclusion signal smearing). This means that a second host interval set after the host-inclusion mixed signal interval negatively affects the quality of the deconvolution as it wrongfully overestimates the host contribution (Figure 8c), unless a very long inclusion interval is chosen which results in increased limits of detection (Pettke et al., 2012).

For quantification of the host, the stochiometric Si content of quartz (46.74 wt%) was used for internal standardization for both GSD-1G and Sca17 brackets. A salinity of 14.25 wt% NaCl equivalent was recalculated to a Cl mass fraction of 86440.5 µg g^{-1}, which was used as the internal standard for the initial quantification step of the FI using the scapolite reference material Sca17 (Figure 8d). This first step is critical because Sca17 has a well-characterized Cl content of ~2.9 % m/m (Seo et al., 2011), whereas GSD-1G contains only ~145 µg g^{-1} Cl, which is too low for reliable quantification due to interferences affecting ^{35}Cl. Chlorine interferences affecting the FI signal are removed by the host-inclusion signal deconvolution procedure. In contrast, quantification using GSD-1G is essential for most elements of interest (e.g. alkali metals, alkaline earth metals, transition metals, REEs), as these elements are not sufficiently characterized or simply of too low mass fractions in Sca17 but are well constrained in GSD-1G. Therefore, a sequential quantification approach is required. In the first step, Na mass fractions of the FI were quantified using Sca17 as CAL and Cl as internal standard. In the second step, these Na mass fractions so calculated for each inclusion individually were used as internal standards for quantification using GSD-1G, enabling robust quantification of all remaining elements of interest in the inclusion.

The chemical composition of the FI indicates the presence of a single dominant, homogeneous fluid, suggesting a major fluid infiltration event during quartz growth. However, e.g., Cu shows notably higher variability (Figure 8e). A comprehensive interpretation of the dataset is provided in Arnold (2022).

2.3. Parallel quantification of melt inclusions

Data from melt inclusions (MI) in mafic, intermediate, and felsic magmas, measured at the University of Bern and published by Chang et al. (2024, 2025), are used to demonstrate parallel inclusion quantification using two internal standards and multiple calibrators. The LA-ICP-MS measurement conditions are outlined in Chang et al. (2024).

Individual MI were analyzed in mineral hosts olivine, clinopyroxene, plagioclase and quartz from magmatic ore-forming systems (Figure 9). These analyses thus provide direct insight into pre-eruptive magma compositions, volatile contents, and the behavior of trace elements during magmatic differentiation. Together, the data allow reconstruction of magma chemistry and crystallization histories, offering a window into the processes that control metal transport and accumulation in magmatic systems prior to magmatic-hydrothermal ore formation.

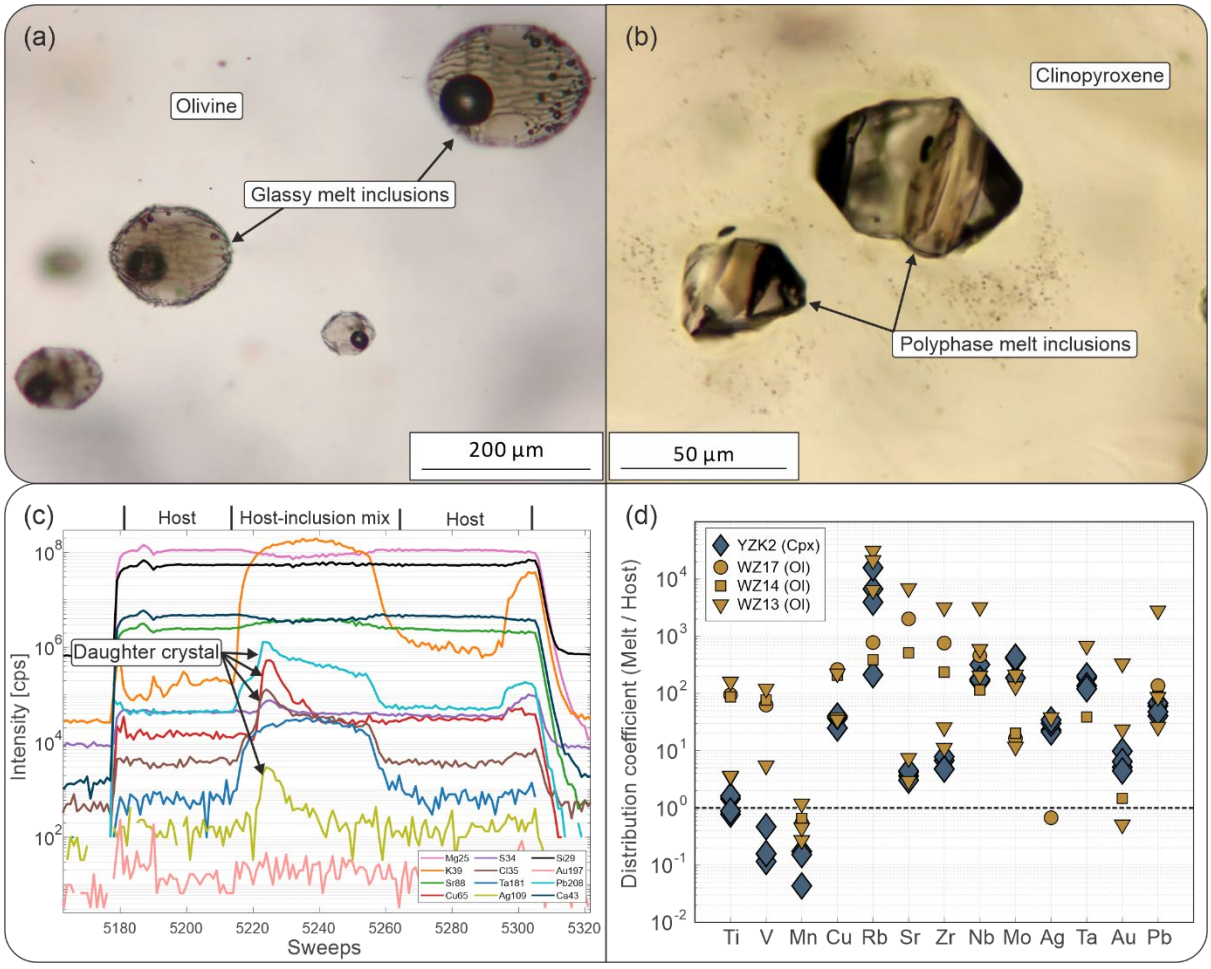

Figure 9: (a) Photomicrograph of glassy melt inclusions in olivine from Vulcano, Italy. (b) Fully crystallized polyphase melt inclusions in clinopyroxene from Two Buttes, USA. Panels (a) and (b) are modified after Chang et al. (2004). (c) Representative intensity signal of a polyphase melt inclusion hosted in clinopyroxene from sample YZK2 (Jianchuan, China). (d) Calculated distribution coefficients for selected trace elements based on individual inclusion-host mineral pairs.

Selected MI measurements published in Chang et al., (2024, 2025) were recalculated here using ICP-Base. GSD-1G was employed as CAL, and two single brackets were measured on two consecutive days. As all analyzed host minerals are nominally H_2O-free, internal standardization used 100 wt% total oxides. For host–inclusion mixed-signal deconvolution and MI quantification, two internal standards were defined for each host phase. In clinopyroxene- and olivine-hosted MI, Si and Al were applied for internal standardization, whereas plagioclase- and feldspar-hosted MI were standardized using Si and Fe. Quartz-hosted MI were quantified using Al and Na as internal standards. The corresponding values are provided in the supplementary material of Chang et al., (2025).

Because both the host mineral and the melt inclusion were quantified for each analysis, melt/host distribution coefficients can be directly compared across different samples and host phases. The four polyphase melt inclusions hosted in clinopyroxene display consistent distribution coefficients, whereas olivine-hosted inclusions show greater variability (Figure 9d). These data illustrate that most analyzed elements preferentially partition into the melt.

2.4. Moving average smoothing and quantification of a line scan on stalagmite MSL-A

To demonstrate the moving average smoothing and quantification feature, a line scan on sample MSL-A from Hulu Cave (Wang et al., 2001) was acquired at the University of Bern. “MSL-A” refers to the section of stalagmite MSL situated between 369 and 435 mm depth from the tip. The Hulu cave is part of a karst system with a high degree of responsivity to shifts in environmental conditions outside the cave (e.g., Cheng et al., 2018; Duan et al., 2018; Kong et al., 2005). A detailed description of the analysis parameters can be found in the supplementary material (Table S2).

One line scan was bracketed by calibrator SRM 612. Moving average windows were configured to span five sweeps with a step size of one sweep per window (Figure 10a). Using this moving average feature the single line scan was effectively separated into 3442 individual integration intervals. Each interval represents a five-sweep segment and was treated analogously to an individual spot analysis but offering a ~10 µm resolution along the scan direction. For internal standardization, the stoichiometric Ca content of calcite (40.04 wt%) was assigned to every segment.

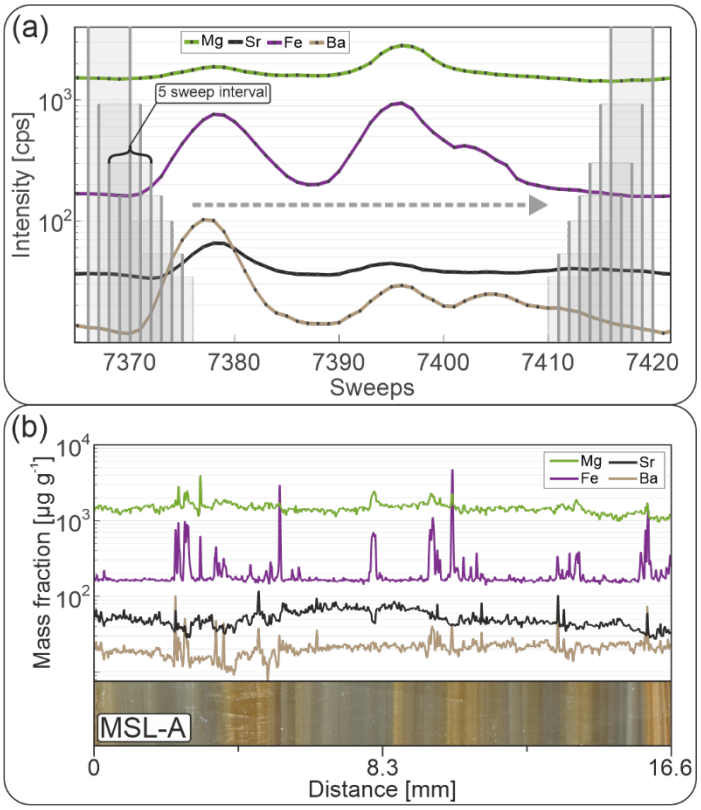

Figure 10: (a) Background-corrected intensities plotted over time (analogous to Figure 8c), illustrating the rolling-average interval selection. The grey shaded areas represent consecutive 5-sweep rolling-average intervals, each shifted forward by one sweep. The grey dashed arrow indicates that this procedure is applied continuously over the entire length of the line scan. (b) Mass fractions plotted as a function of distance along stalagmite MSL-A. A high-resolution scan of the sample is included to correlate visible growth layers with corresponding variations in analyte mass fraction.

To demonstrate the applicability of our data processing approach, we focus on Mg, Ba, Sr, and Fe, selected for their compatibility with calcite and incorporation into the stalagmite matrix (Wassenburg et al., 2020). The results show coherent variability along the transect (Figure 10b), with Mg, Fe, and Ba displaying strongly correlated peaks. Sr and Ba also coincide in some intervals but do not consistently align with Mg and Fe. This likely reflects differences in partitioning during calcite precipitation and/or changes in hydrological pathways (Wassenburg et al., 2020; Treble et al., 2022).

3. ICP-Base as a foundation for community-driven development

The modular design, comprehensible data architecture, and open-source code of ICP-Base enable easy reuse of existing modules to develop new workflows (Figure 1). For example, a geochronology or stable

isotope routine can be implemented with minimal effort, as data import for common ICP-MS instruments and key processing steps (e.g., interval selection, classification) are already established or largely analogous. As a result, researchers can focus on developing the main features of their new application without spending considerable time on initial setup and conceptualization. These new routines can be integrated into the centralized database, enabling direct comparison and joint evaluation of different data types. This also enables the implementation of split-stream workflows (e.g., parallel processing of quantification and geochronology data).

4. Conclusion

ICP-Base streamlines LA-ICP-MS data processing by combining transparent quantification routines, integrated data evaluation, and direct visualization within a single software environment. As a free and open-source application, it is accessible to the entire community and does not require a MATLAB® license for usage. The software can be used for quantification of mineral spot analyses, fully enclosed solid and fluid inclusions, as well as line scan data. Its centralized data organization allows users to evaluate quantification results from individual measurement sessions as well as to compare results across multiple sessions over long time periods. ICP-Base maintains the full analytical context through its centralized database, enabling straightforward long-term reproducibility tests and continuous monitoring of LA-ICP-MS system performance. The integration of the VisModule from MinPlotX (Walters and Gies, 2025) enables users to perform comprehensive data visualization and generate publication-ready figures directly within the software environment, minimizing the need for external plotting tools. Beyond its immediate capabilities, ICP-Base establishes a foundation for community-driven development. Owing to its modular design and structured data architecture, existing modules can be reused and expanded to implement new workflows without rebuilding core functionality. ICP-Base therefore not only provides a robust solution for current quantification challenges, but also represents an extensible framework and basis for future development in LA-ICP-MS data processing.

5. Acknowledgements

D. Rufer and J. Dietrich are gratefully acknowledged for fruitful discussions and for their encouragement throughout the programming process. J. Chang, T. Arnold, S. Thurnherr, and A. Paine are thanked for

allowing the use of their measurements for the application examples and for helpful discussions about the data. R. Tamblyn, D. Toro Vivanco, T. Markmann, P. Lanari and F. Neidhart are acknowledged for their valuable ideas, help and constructive feedback.

Code availability section

Name of the code/library: ICP-Base

Contact: sebastian.stumpf@unibe.ch

Program language: MATLAB®

Software required: None for compiled versions, MATLAB® 2021b for non-compiled versions

The source codes and binaries are available for downloading at:

https://github.com/GeoSebastianStumpf/ICP-Base

References

Altenberger F., Krause J., Auer T., Auer A., Berndt J., 2024. G.O.Joe: A New Non-Commercial Software Tool for the Processing of LA-ICP-MS Trace Element Data. Geostandards and Geoanalytical Research 49, 281-294.

Arnold T., 2022. The Spittallamm-cleft: A Testimony of Fluid Circulation in Exhuming Orogens. Master Thesis, University of Bern.

Audétat A., Günther D., Heinrich C.A., 1998. Formation of a Magmatic-Hydrothermal Ore Deposit: Insights with LA-ICP-MS Analysis of Fluid Inclusions. Science 279, 2091-2094.

Branson O., Fehrenbacher J.S., Vetter L., Sadekov A.Y., Eggins S.E., Spero H.J., 2019. *LAtools*: A data analysis package for the reproducible reduction of LA-ICPMS data. Chemical Geology 504, 83-95.

Bretscher A., Hermann J., Pettke T., 2018. The influence of oceanic oxidation on serpentinite dehydration during subduction. Earth and Planetary Science Letters 499, 173-184.

Chang J., Audétat A., Pettke T., 2024. The gold content of mafic to felsic potassic magmas. Nature Communications 15, 6988.

Chang J., Audétat A., Pettke T., 2025. Ten kilometers ascent of porphyry Cu (Au, Mo)-forming fluids in the Sanjiang region, China. Nature Communications 16, 2330.

Chang J., Audétat A., Pettke T., 2025. Ten kilometers ascent of porphyry Cu (Au, Mo)-forming fluids in the Sanjiang region, China. Nature Communications 16, 2330.

Cheng H., Edwards R.L., Southon J., Matsumoto K., Feinberg J.M., Sinha A., Zhou W., Li H., Li X., Xu Y., Chen S., Tan M., Wang Q., Wang Y., Ning Y., 2018. Atmospheric $^{14}C/^{12}C$ changes during the last glacial period from Hulu Cave. Science 362, 1293-1297.

Duan F., Wu J., Wang Y., Edwards R.L., Cheng H., Kong X., Zhang W., 2015. A 3000-yr annually laminated stalagmite record of the Last Glacial Maximum from Hulu Cave, China. Quaternary Research 83, 360-369.

Faltusová V., Vaculovič T., Holá M., Kanický V., 2022. Ilaps – python software for data reduction and imaging with LA-ICP-MS. Journal of Analytical Atomic Spectrometry 37, 733-740.

Guillong M., Meier D.L., Allan M.M., Heinrich C.A., Yardley B.W.D., 2008. Appendix A6: SILLS: A MATLAB-based program for the reduction of laser ablation ICP-MS data of homogeneous materials and inclusions. In: Sylvester, P. (Ed.) Laser Ablation ICP-MS in the Earth Sciences: Current Practices and Outstanding Issues, Mineralogical Association of Canada, Short Course Series 40, 328-333.

Günther, D., Audétat A., Frischknecht R., Heinrich C.A., 1998. Quantitative analysis of major, minor and trace elements in fluid inclusions using laser ablation– inductively coupled plasma mass spectrometry. Journal of Analytical Atomic Spectrometry 13, 263-270.

Halter W.E., Pettke T., Heinrich C.A., Rothen-Rutishauser B., 2002. Major to trace element analysis of melt inclusions by laser-ablation ICP-MS: methods of quantification. Chemical Geology 183, 63-86.

Heinrich W.A., Pettke T., Halter W.E., Aigner-Torres M., Audétat A., Günther D., Hattendorf B., Bleiner D., Guillong M., Horn I., 2003. Quantitative multi-element analysis of minerals, fluid and melt inclusions by laser-ablation inductively-coupled-plasma mass-spectrometry, Geochimica et Cosmochimica Acta 67, 3473-3496.

Kong X., Wang Y., Wu J., Cheng H., Edwards R.L., Wang X., 2005. Complicated responses of stalagmite $\delta^{13}C$ to climate change during the last glaciation from Hulu Cave, Nanjing, China. Science in China Series D: Earth Sciences 38, 2174-2181.

Lanari P., Vidal O., De Andrade V., Dubacq B., Lewin E., Grosch E.G., Schwartz S., 2014. XMapTools: A MATLAB©-based program for electron microprobe X-ray image processing and geothermobarometry. Computers & Geosciences 62, 227-240.

Markmann A.T., Lanari P., Piccoli F., Pettke T., Tamblyn R., Tedeschi M., Lueder M., Kunz B.E., Riel N., Laughton J., 2024. Multi-phase quantitative compositional mapping by LA-ICP-MS: Analytical approach and data reduction protocol implemented in XmapTools. Chemical Geology 646, 121895.

Mischel S.A., Mertz-Kraus R., Jochum K.P., Scholz D., 2017. TERMITE: An R script for fast reduction of laser ablation inductively coupled plasma mass spectrometry data and its application to trace element measurements. Rapid Communications in Mass Spectrometry 31, 1079-1087.

Pettke T., Oberli F., Audétat A., Guillong M., Simon A.C., Hanley J.J., Klemm L.M., 2012. Recent developments in element concentration and isotope ratio analysis of individual fluid inclusions by laser ablation single and multiple collector ICP-MS. Ore Geology Reviews 44, 10-38.

Pettke T., Bretscher A., 2022. Fluid-mediated element cycling in subducted oceanic lithosphere: The orogenic serpentinite perspective. Earth Science Reviews 225, 103896.

Stucki A., 2001. High grade Mesozoic ophiolites of the Southern Steep Belt, Central Alps. Dissertation No. 14206, ETH Zürich.

Treble P.C., Baker A., Abram N.J., Hellstrom J.C., Crawford J., Gagan M.K., Borsato A., Griffiths A.D., Bajo P., Markowska M., Priestley S.C., Hankin S., Paterson D., 2022. Ubiquitous karst hydrological control on speleothem oxygen isotope variability in a global study, Nature Communications Earth & Environment 3, 29.

Thurnherr S., 2025. Genesis and Alpine Metamorphic History of the Gana Rossa Metaperidotite Body, Graubünden, Unveiled by Geological Mapping, Petrology, and Geochemistry. Master Thesis, University of Bern.

Vieira Duarte. J.F., Piccoli F., Pettke T., Hermann J., 2021. Textural and Geochemical Evidence for Magnetite Production upon Antigorite Breakdown During Subduction. Journal of Petrology 62, 1-29.

Vieira Duarte J.F., Pettke T., Hermann J., Piccoli F., 2023. Oxide-silicate petrology and geochemistry of subducted hydrous ultramafic rocks beyond antigorite dehydration (Central Alps, Switzerland). Contributions to Mineralogy and Petrology 178, 60.

Walters J.B., Gies N.B., 2025. MinPlotX: A powerful tool for formula recalculation, visualization, and comparison of large mineral compositional datasets. Mineralogia 56, 13-22.

Wang Y.J., Cheng H., Edwards R.L., An Z.S., Wu J.Y., Shen C.C., Dorale J.A., 2001. A High-Resolution Absolute-Dated Late Pleistocene Monsoon Record from Hulu Cave, China. Science 294, 2345-2348.

Wassenburg J.A., Riechelmann S., Schröder-Ritzrau A., Riechelmann D.F.C., Richter D.K., Immenhauser A., Terente M., Constantin S., Hachenberg A., Hansen M., Scholz D., 2020. Calcite Mg and Sr partition

coefficients in cave environments: Implications for interpreting prior calcite precipitation in speleothems. Geochimica et Cosmochimica Acta 29, 581-596.

Supplementary Materials

Table S1 Analytical conditions for LA-ICP-MS mineral analyses for ultramafic samples

Laboratory and Sample Preparation	
Laboratory name	Insitute of Geological Sciences, University of Bern, Switzerland
Sample type/mineral	Olivine, Orthopyroxene, Chlorite
Sample preparation	Thick section (~70 µm thickness). Final polishing with 1 µm diamond paste.
Laser ablation system	
Instrument	Resonetics RESOlutionSE excimer laser
Cell type	Laurin Technic S155 constant volume, dual volume ablation cell
Laser wavelength	193 nm
Fluence	4 J/cm^2
Sampling mode	Single hole drilling, circular shape
Pre-ablation cleaning	One sizer bigger than measurement beam
Spot diameter (nominal)	50, 64, 80 µm
Repetition rate	10 Hz
Ablation duration	40 s
Carrier gas	He mixed with N_2
He gas flow rate	0.40 L/min
N_2 gas flow rate	0.003 L/min
Ar mix gas flow rate	0.86 L/min
Oxide production rate ThO/Th	<0.20 %
ICP Mass Spectrometer	
Instrument	Agilent 7900 quadrupole
Sample introduction	Ablation aerosol only
RF power	1550 W
Monitored masses	^{7}Li, ^{9}Be, ^{11}B, ^{23}Na, ^{25}Mg, ^{27}Al, ^{29}Si, ^{31}P, ^{39}K, ^{43}Ca, ^{45}Sc, ^{49}Ti, ^{51}V, ^{53}Cr, ^{55}Mn, ^{57}Fe, ^{59}Co, ^{61}Ni, ^{62}Ni, ^{65}Cu, ^{66}Zn, ^{75}As, ^{85}Rb, ^{88}Sr, ^{89}Y, ^{90}Zr, ^{93}Nb, ^{95}Mo, ^{98}Mo, ^{109}Ag, ^{111}Cd, ^{115}In, ^{118}Sn, ^{121}Sb, ^{133}Cs, ^{137}Ba, ^{139}La, ^{140}Ce, ^{141}Pr, ^{146}Nd, ^{147}Sm, ^{151}Eu, ^{157}Gd, ^{159}Tb, ^{163}Dy, ^{165}Ho, ^{167}Er, ^{169}Tm, ^{173}Yb, ^{175}Lu, ^{178}Hf, ^{181}Ta, ^{182}W, ^{208}Pb, ^{209}Bi, ^{232}Th, ^{238}U
Tuning	Line scan on NIST SRM 612 glass with a beam size of 50 µm, a scanning speed of 5 µm/s, and a fluence of 2.5 J/m²
Analysis mode	Time Resolved Analysis
Integration time for single data point	10 ms except 20 ms for ^{39}K, ^{75}As, ^{121}Sb, ^{139}La, ^{140}Ce, ^{141}Pr, ^{182}W, ^{208}Pb and 30 ms for ^{11}B and ^{238}U

Table S2: Analytical conditions for LA-ICP-MS linescans of stalagmite MSL-A

Laboratory and Sample Preparation	
Laboratory name	Insitute of Geological Sciences, University of Bern, Switzerland
Sample type/mineral	Calcite
Sample preparation	
Laser ablation system - Tuning	
Instrument (Tuning)	Resonetics RESOlutionSE excimer laser
Cell type (Tuning)	Laurin Technic S155 dual volume ablation cell
Laser wavelength	193 nm
Material	NIST SRM612
Fluence	2.5 J/cm^2
Sampling mode	Linescan 5 µm/s
Pre-ablation cleaning	Lincescan (64 µm diameter)
Spot diameter (nominal)	50 µm
Repetition rate	10 Hz
Carrier gas	He mixed with N_2
He gas flow rate	0.40 L/min
N_2 gas flow rate	0.003 L/min
Ar mix gas flow rate	0.86 L/min
Oxide production rate ThO/Th	<0.20 %
Laser ablation system - Analyses	
Instrument (Analyses)	Resonetics RESOlutionSE excimer laser
Cell type (Analyses)	Laurin Technic S155 constant volume, dual volume ablation cell
Laser wavelength	193 nm
Fluence	3 J/cm^2
Sampling mode	Linescan 14 µm/s
Pre-ablation cleaning	50 µm spot size linescan at 25% spot overlap
Spot diameter (nominal)	38 µm
Repetition rate	10 Hz
Carrier gas	He mixed with N_2
He gas flow rate	0.40 L/min
N_2 gas flow rate	0.003 L/min
Ar mix gas flow rate	0.86 L/min
Oxide production rate ThO/Th	<0.20 %
ICP Mass Spectrometer	
Instrument	Agilent 7900 quadrupole ICP-MS

Sample introduction	Ablation aerosol only
RF power	1550 W
Monitored masses	^{23}Na, ^{25}Mg, ^{27}Al, ^{29}Si, ^{31}P, ^{34}S, ^{43}Ca, ^{49}Ti, ^{51}V, ^{55}Mn, ^{57}Fe, ^{59}Co, ^{65}Cu, ^{66}Zn, ^{85}Rb, ^{88}Sr, ^{89}Y, ^{90}Zr, ^{111}Cd, ^{133}Cs, ^{137}Ba, ^{139}La, ^{140}Ce, ^{146}Nd, ^{173}Yb, ^{175}Lu, ^{208}Pb, ^{232}Th, ^{238}U
Analysis mode	Time Resolved Analysis
Integration time for single data point	20 ms except 30 ms for ^{27}Al, ^{29}Si, ^{34}S, ^{31}P, ^{208}Pb